Chapter-2

EQUILIBRIUM SOLAR PLASMA PROPERTIES IN THE POLYTROPIC TURBOMAGNETIC GES-MODEL FABRIC

Abstract: *The idealistic GES-model based solar plasma system is re-examined with proper inclusion of the realistic solar-plasma structuring key factors. It incorporates the non-thermal (κ-distributed) electron population, global magnetic field, and solar plasma fluid turbulence. The necessary basic governing equations are developed in a rectified form for both the SIP and SWP regions. Various key equilibrium properties of the system are explored graphically by numerical analysis of the model equations. The outcomes on this new model are compared with the previously reported widely accepted SSM results*[†].

2.1 INTRODUCTION

The Sun and its ambient atmosphere have been a complex dynamic plasma system yet to be well investigated. One of such less-explored characteristics is the population of non-thermally distributed solar plasma constituents that has been confirmed by the diversified observational techniques, and their role in the overall plasma structure evolutionary processes [1-3]. It is extensively found in the literature that the investigation of coupling dynamics of the Sun and its atmosphere has considerably been performed on the basis of various theoretical model formalisms in the past [4]. Up to the year 1958, it has been assumed that the structure of the solar atmosphere, so-called the corona is maintained in hydrostatic equilibrium by the Sun's gravitational field. The first non-isothermal model for the solar corona has been developed by Chapman in 1957 on the basis of basic principles of hydrostatics [5]. The density profile variation reported therein has indicated convectively unstable nature of the solar hydrostatic equilibrium. Although the presence of turbulence behind such instability has been argued on, the non-equilibrium continuously expanding solar atmosphere has never been clearly apprehended that was confirmed later on by sufficient in situ measurements [6, 7]. It has also been found based

[†]Sarma, P. and Karmakar, P. K. Solar plasma characterization in Kappa (κ)-modified polytropic turbomagnetic GES-model perspective. *Monthly Notices of the Royal Astronomical Society*, 519(2):2879-2916, 2023.

on the same model later that the kinetic pressure and density predicted therein have superseded the respective quantities in the interstellar medium [8, 9].

Eugene Parker in 1958 has formulated the first hydrodynamic model of the solar corona revealing satisfactorily the continuous hot coronal mass expansion into the interplanetary cold space extending up to infinity [8]. It has assumed spherical symmetry of the Sun in accordance with the standard solar model (SSM). The basic physics behind this Parker model for the continuous outflow of the existing solar wind particles is the large kinetic pressure gradient accelerating the coronal plasma from the subsonic to supersonic/hypersonic flow in accordance with the de Laval nozzle effect over varying cross-section [10]. Although, this model has been successful in explaining several fundamental issues of the solar wind dynamics; key limitations of the same have, however, been realized later on. For example, this model has failed to explain the high-speed origin of the solar wind (even at a distance of 1 au), as widely observed, without the help of any supplementary coronal heating source. Besides, it has not considered the ambipolar space charge electrodynamical effects associated with the magnetized diffused solar wind medium [8, 11, 12].

It has been recognized later in 1960 that the solar wind plasma (SWP) becomes almost collision less in most of the regions in the interplanetary space. Consequently, the associated velocity distribution deviates from the Maxwellian one [9]. Chamberlain in 1960 has proposed the first exospheric model for the solar wind with a fully kinetic treatment, founded on the invariants of constitutive particles derived fundamentally from the Jeans theory of planetary exospheres, also known as the solar breeze model [13]. Though this model has been successful in omitting the extra coronal plasma heating source as required in the Parker solar model, the bulk velocity as predicted by the exospheric solar breeze solution appears to be much too small compared to those observed by the first interplanetary missions at 1 au. Moreover, the proton density and temperature at 1 au as predicted by this model have been found to be quite different from the direct measurements in the interplanetary space, as performed in 1962 and later [6, 7, 9]. A number of remarkable modifications have been actualized in the next-generation kinetic exospheric models for refinements. It has still been lacking in an adequate description of the solar wind flow dynamics. More particularly, one can say that all the relevant kinetic processes of the solar wind near and below the exobase have since then been remaining ill-understood despite the above-mentioned ameliorations in explorative approaches [9, 14-16].

In this direction of solar wind exploration, it is inevitably noteworthy that the gravito-electrostatic sheath (GES)-model has been well successful from the rest of the reported models in explaining the surface origin of the SWP by the dynamic conversion of the solar interior plasma (SIP) through the diffuse interfacial solar surface boundary (SSB). The SSB has been uniquely defined and characterized with the help of the exact gravito-electrostatic force balancing condition [17-22]. The original GES-model is based on the idealistic field-free plasma environments composed of the Boltzmann (thermal) electrons and inertial (hydrodynamic) ions [17]. Clearly, the novelty of the proposed GES analysis exists in the unique treatment of the collective plasma effects (in the form of plasma–wall interaction processes) herein against the rest of the existing solar models including the exospheric ones. But, the presence of non-thermal plasma electrons, as confirmed extensively by the diversified astronomical observations [23, 24], motivates us to refine the previous GES-model so as to see the electronic non-thermality effects on the solar plasma evolution and re-structurization. Another driving force behind mobilizing this investigation is in the fact inherent in the frustrated Debye shielding in non-thermal plasmas [25, 26]. In other words, the collective screening effects (Debye shielding) in non-thermal plasmas are highly affected (frustrated) by the non-Boltzmann electrons [25, 26]. In terms of exact mathematical expressions, the κ-modified Debye shielding scale length ($\lambda_{D,\kappa}$) in non-Maxwellian plasmas maps that ($\lambda_{D,M}$) in the Maxwellian plasmas (in generic notations) explicitly given as $\lambda_{D,\kappa} = \lambda_{D,M}\left[(\kappa-1.5)/(\kappa-0.5)\right]^{1/2}$. As a consequence of the non-thermal effects, the Debye screening scale length, and hence, the plasma sheath width in the non-thermal (non-Maxwellian) plasmas are shorter than those in the thermal (Maxwellian) plasmas [25, 26]. It stimulates the inclusion of the κ-modified thermo-statistics extremely relevant in non-thermal solar plasmas to see the new GES structure.

It is worth mentioning that a systematic study in the above direction has already been executed on a non-polytropic GES-model picture in a turbulent non-magnetic plasma environment [22]. The non-thermal microphysical aspects of the electronic dynamics, however, still remain a great challenge in the solar plasma scenarios. The presented study is indeed a continued exploration driven motivationally by the current observational scenarios [4, 27]. It could be relevantly applied to the κ-modified polytropic GES-model picture on turbulent magneto-active plasma fluid equilibrium in any type of stellar plasma configurations. Besides, the analysis could be broadly useful to

characterize the entire equilibrium structure composed of the bounded SIP and the unbounded SWP coupled via a modified SSB in the non-thermal solar plasma viewpoint of the realistic astronomic importance. In brief the novelty and significance of the presented study can be outlined as follows. This GES centric exploration considers the application of the rudimentary laboratory-scaled plasma sheath formation physics in the solar plasma dynamics with realistic electron non-thermality effects. The new model governing equations incorporate the major sensible solar plasma structuring key factors jointly. It includes the non-thermal electronic thermo-statistics, global magnetic field, and plasma-fluidic turbulence effects. A thorough characterization of the equilibrium structure of the entire solar plasma system is systematically carried out. All the obtained results based on our model analysis are compared with the relevant results from the previous solar study widely available in the literature, for the reliability check-up and appropriate validation of our present analysis.

2.2 SOLAR PLASMA MODEL FORMULATION

We consider the solar constitutive plasma medium to be composed of non-thermal lighter non-gravitating κ-distributed electrons and heavier inertial gravitating ions throughout the entire solar plasma system. The consideration of a spherically symmetric model configuration makes all the relevant physical variables here to have only radial dependency (1D) with the polar and azimuthal geometric counterparts fully relaxed [28, 29]. The plasma constitutive electrons and ions form a quasi-neutral homogeneous equilibrium. The magneto-active solar plasma medium is turbulent in nature, modelled with the Larson logatropism [30]. This is because of the fact that logatropic and polytropic equations of state are well known to yield more accurate results in the context of diverse astrophysical structures. The anisotropy aspects in the temperature distribution [3, 31, 32] are ignored here for analytic simplicity.

The lighter electrons are capable of easily flying away from the plasma self-gravitational potential barrier that cannot be overcome by the background lying fluidic inertial ions. This fact is evident from the gravito-thermal coupling estimation for both the electronic and the ionic species in the solar plasma system [17, 18]. This is the basic phenomenon of space charge polarization under the self-gravity action responsible for the development of our modified GES-model. All other basic physical insights behind the formulation of the original GES-model fabric [17, 18, 21] are well retained here as well. It is to be noted here that our considered global quasi-neutrality condition ($N_e \approx N_i$

= *N*) is justified by the negligible magnitude of the ratio of the solar plasma electron Debye length to the Jeans length required for the description of the solar plasma system. The macroscopic plasma quasi-neutrality condition, however, might not be fulfilled locally in the presence of inhomogeneous plasma-boundary wall interaction processes on the micro-scales despite being less sensible on the astrophysical scales of space and time. With all these reservations in our proposed model, we proceed to explore the key equilibrium solar plasma characteristics based on our thermo-statistically modified GES-model formalism in this study.

2.2.1 SIP GOVERNING EQUATIONS

The basic governing equations describing the bounded SIP scale consist of the thermo-statistical electron distribution law, ion continuity equation, ion momentum equation, bulk fluidic equation of state, electrostatic Poisson equation, gravitational Poisson equation, and electric current density evolution equation in customary notations in a closed form [17, 21, 22]. The electron population is accordingly governed by the Kappa (κ) distribution, which is basically a generalized Lorentzian κ-density distribution law with the thermo-statistical spectral index κ (= $(q-1)^{-1}$, q : entropic index), given in all generic symbols [1, 2, 23] as

$$n_e = n_0\left[1-\left(\kappa-\frac{3}{2}\right)^{-1}\frac{e\phi}{k_B T_0}\right]^{-\kappa+1/2}. \tag{2.1}$$

It is to be noted here that the spatiotemporal differential operators in the defined coordination space (r, t) are represented respectively as $d_r = d/dr$ and $d_t = d/dt$; and so forth. The ion continuity equation in usual symbolism with linear spatiotemporal operators in contracted form is given as

$$\partial_t n_i + v\left(\partial_r n_i\right) + n_i\left(\partial_r v\right) + \left(\frac{2}{r}\right) n_i v = 0. \tag{2.2}$$

The ion momentum equation is expressed as

$$m_i n_i\left[\partial_t v + v\left(\partial_r v\right)\right] = -e n_i\left(\partial_r \phi\right) - \partial_r P_T - m_i n_i\left(\partial_r \psi\right) + \eta\left(\frac{1}{r^2}\right)\partial_r\left(r^2 \partial_r v\right). \tag{2.3}$$

The modified equation of state developed after inclusion of the realistic solar plasma parametric effects as mentioned above is expressed explicitly as

$$P_T = \alpha n_0^{\Gamma}\left[1-\left(\frac{2}{2\kappa-3}\right)\frac{e\phi}{k_B T_0}\right]^{(-\kappa+1/2)\Gamma} + P_{Th}\left[1+ln\left(\frac{n_i}{n_0}\right)\right]+\frac{B^2}{2\mu_0}. \quad (2.4)$$

Here, the first term represents the pressure caused by the non-thermal electrons. The second term stands for ion thermal pressure and the fluid pressure due to turbulence. The final term expresses the magnetic pressure, which is effective under a global approach. Here, α stands for the non-thermally modified polytropic constant signifying the pressure-density correlation in the non-thermal solar plasmas. Similarly, $\Gamma = (2\kappa + 5)/(2\kappa + 3)$ is the κ-modified polytropic exponent [23, 31], which typifies the thermo-statistical state of the adopted macroscopic plasma. The electrostatic Poisson equation describing the electrostatic potential (φ) distribution due to charge density fields (en_e and en_i) associated with the constitutive electronic and ionic species is cast as

$$\partial_r^2\phi+\left(\frac{2}{r}\right)\partial_r\phi=\frac{e}{\varepsilon_0}\left(n_e-n_i\right). \quad (2.5)$$

The self-gravitational Poisson equation describing the gravitational potential (ψ) distribution sourced in the SIP material density field ($m_i n_i$) is expressed in the generic notations as

$$\partial_r^2\psi+\left(\frac{2}{r}\right)\partial_r\psi=4\pi G\left(m_i n_i\right). \quad (2.6)$$

We close our basic model equations by incorporating the electric current density evolution derived in the same customary notations [21, 22] as given below:

$$j_{SIP}=n_i e\left[-\sqrt{2r\left(\partial_r\psi\right)}-\sqrt{\left(\frac{2e}{m_i}\right)r\left(\partial_r\phi\right)}\right]+n_e e\sqrt{\left(\frac{2e}{m_e}\right)r\left(\partial_r\phi\right)}. \quad (2.7)$$

In the above equation, the first and the second terms represent the contributions of the heavier gravitating ions and the lighter electrons to the effective SIP current density, respectively. The physical significances of the symbols in the above equations are clearly mentioned in Table 2.1.

Table 2.1: Symbols and their significances

S. No.	Symbol	Significance
1	$n_{e(i)}$	Electron (ion) number density
2	n_o	Mean SIP equilibrium number density
3	e	Magnitude of electronic (ionic) charge

4	k_B	Boltzmann constant, k_B=1.38×10^{-23} J K^{-1}.
5	T_o	SIP core temperature
6	v	Local ionic flow speed
7	$m_{e(i)}$	Mass of electron (ion)
8	P_T	Total pressure in a considered region
9	η	Shear viscosity coefficient of the SIP fluid
10	P_{Th}	Bulk plasma thermal pressure
11	B	Effective magnetic field responsible for the magnetic pressure
12	μ_0	Vacuum permeability
13	ε_0	Vacuum permittivity
14	G	Newtonian universal gravitational constant, G=6.67×10^{-11} N m^2 kg^{-2}

To proceed forward to numerically characterize the equilibrium structure of the Sun, we express the above fundamental SIP governing equations in the normalized time-stationary form. The astronomically relevant normalization scheme is put in Table 2.2. Accordingly, the normalized forms of equations (2.1) - (2.5) are expressed as

$$N_e = \left[1-\left(\frac{2}{2\kappa-3}\right)\Phi\right]^{-\kappa+1/2}, \tag{2.8}$$

$$M\left(\partial_\xi N\right)+N\left(\partial_\xi M\right)+\left(\frac{2}{\xi}\right)M\,N=0, \tag{2.9}$$

$$M\left(\partial_\xi M\right)=-T_e^*\left(\partial_\xi\Phi\right)-\left(\frac{\alpha\lambda_J\Gamma n_0^{\Gamma-1}}{m_i c_s^2}\right)N^{\Gamma-2}\left(\frac{2\kappa-1}{2\kappa-3}\right)\left[1-\left(\frac{2}{2\kappa-3}\right)\Phi\right]^{-\kappa-1/2}\frac{1}{\lambda_J}\left[\partial_\xi\Phi+T_e^*\Phi\,\partial_\xi\left(\frac{1}{T_e^*}\right)\right], \tag{2.10}$$

$$-\frac{1}{N}\left[T_i^*\left(\partial_\xi N\right)+N\left(\partial_\xi T_i^*\right)\right]\left[1+\ln(N)\right]-T_i^*\frac{1}{N}\left(\partial_\xi N\right)-\partial_\xi\Psi+\left(\frac{\eta}{m_i n_0 c_s\lambda_J}\right)\frac{1}{\xi^2}\frac{1}{N}\left[\partial_\xi\left(\xi^2\,\partial_\xi M\right)\right]$$

$$P_T^*=\left(\frac{\alpha\,n_0^\Gamma}{P_0}\right)\left[1-\left(\frac{2}{2\kappa-3}\right)\Phi\right]^{(-\kappa+1/2)\Gamma}+P_{Th}^*\left[1+ln\left(N_i\right)\right]+\beta_0\left(B^*\right)^2, \tag{2.11}$$

$$N_e-N_i=\left(\frac{\lambda_{De}}{\lambda_J}\right)^2\left[\partial_\xi^2\Phi+\left(\frac{2}{\xi}\right)\partial_\xi\Phi\right]. \tag{2.12}$$

The asymptotic value of $\left(\lambda_{De}/\lambda_J\right)\sim 10^{-20}$ in equation (2.12) justifies the global quasi-neutrality ($N_e\approx N_i=N$) in the entire solar plasma system. Now, the gravitational Poisson equation in the normalized form is expressed as

$$\partial_{\xi}^{2}\Psi+\left(\frac{2}{\xi}\right)\partial_{\xi}\Psi=N\,. \tag{2.13}$$

The normalized SIP current density evolution equation is given by

$$J_{SIP}=N\left[-\sqrt{2\xi\left(\partial_{\xi}\Psi\right)}-\sqrt{\left\{2\left(\frac{T_e}{T_i}\right)\xi\left(\partial_{\xi}\Phi\right)\right\}}+\sqrt{\left\{2\left(\frac{m_i}{m_e}\right)\left(\frac{T_e}{T_i}\right)\xi\left(\partial_{\xi}\Phi\right)\right\}}\right]. \tag{2.14}$$

We now couple the above equations to obtain a basic set of time-stationary first-order differential equations describing the SIP dynamics. After exactly following the original analysis [17], we now apply the fourth-order Runge-Kutta (RK-IV) method for the numerical characterization of the SIP. Here, the net effective magnetic field effects in the considered microfluidic element is negligible. The ignorable cohesive force among the constitutive fluid particles (due to high temperature environment) makes the viscosity effects negligibly small in the analysable scale [28]. Accordingly, the initial and input values for our numerical analysis to run smoothly are offered in Table 2.3 elaborately.

Table 2.2: Normalization scheme

Physical parameter	Normalized symbol (generic)	Normalizing parameter	Typical value
Radial distance (r)	$\xi = r/\lambda_J$	Jeans length (λ_J)	2×10^{8} m
Electron (ion) population density ($n_{e(i)}$)	$N \approx N_{e(i)} = n_{e(i)}/n_0$	Mean SIP equilibrium density (n_0)	10^{30} m^{-3}
Electric potential (ϕ)	$\Phi = e\phi/k_B T_0$	Core electron thermal potential ($k_B T_0/e$)	10^{3} V
Ion speed (v)	$M = v/c_s$	Speed of sound in SIP (c_s)	3×10^{5} m s^{-1}
Gravitational potential (ψ)	$\Psi = \psi/c_s^2$	Square of the sound speed in SIP (c_s^2)	9×10^{10} m^2 s^{-2}
Electron (ion) temperature ($T_{e(i)}$)	$T_{e(i)}^{*} = T_{e(i)}/T_0$	Core temperature (T_0)	10^{7} K
Pressure (P_T)	$P_T^{*} = P_T/P_0$	Mean SIP pressure (P_0)	10^{14} N m^{-2}
Current density ($j_{SIP(SWP)}$)	$J_{SIP(SWP)} = j_{SIP(SWP)}/J_B$	SIP Bohm current density strength (J_B)	4.8×10^{16} A m^{-2}

Table 2.3: Initial and input value

Physical parameter (Relevant for the Sun)	SIP input (Judicious for heliocore)	SWP input (SIP-derived for SSB)
Radius	0.00001	3.5
Gravitational field strength	0.00001	0.6
Electric potential	0.0001	-1.01
Electric field strength	0.0001	-0.6

2.2.2 SWP GOVERNING EQUATIONS

In the SWP scale dynamics, the Sun acts as a point source of gravity of the Newtonian type. As a result, the dynamics of the plasma fluid is governed by the same equations as in the SIP scale, except the solar self-gravity is replaced by the corresponding inverse-square (Newtonian) solar gravity. As a result, the gravitational Poisson equation becomes redundant [17]. Accordingly, the basic governing equations in the same system of symbolism are formulated as follows.

The non-thermal κ-distributed electron population is described by the appropriate thermo-statistical distribution law given as

$$n_e = n_0\left[1-\left(\kappa-\frac{3}{2}\right)^{-1}\frac{e\phi}{k_B T_0}\right]^{-\kappa+1/2}. \tag{2.15}$$

The ion continuity equation is expressed as

$$\partial_t n_i + v\left(\partial_r n_i\right)+ n_i\left(\partial_r v\right)+\left(\frac{2}{r}\right)n_i v = 0. \tag{2.16}$$

The ion momentum equation in presence of the external solar gravity becomes

$$m_i n_i\left[\partial_t v + v\left(\partial_r v\right)\right] = -e n_i\left(\partial_r \phi\right)-\partial_r P_T - m_i n_i\left(\frac{GM_\odot}{r^2}\right)+\eta\left(\frac{1}{r^2}\right)\partial_r\left(r^2\partial_r v\right). \tag{2.17}$$

The modified equation of state for the SWP description is expressed as

$$P_T = \alpha\, n_0^{\Gamma}\left[1-\left(\frac{2}{2\kappa-3}\right)\frac{e\phi}{k_B T_0}\right]^{(-\kappa+1/2)\Gamma}+P_{Th}\left[1+ln\left(\frac{n_i}{n_0}\right)\right]+\frac{B^2}{2\mu_0}. \tag{2.18}$$

The electrostatic Poisson equation for the electric potential distribution is written as

$$\partial_r^2\phi+\left(\frac{2}{r}\right)\partial_r\phi = \frac{e}{\varepsilon_0}\left(n_e - n_i\right). \tag{2.19}$$

The unnormalized electric current density evolution equation in the SWP under the action of external solar gravity in the same customary notations is given as

$$j_{SWP} = n_i e\left[-\sqrt{2r\left(\frac{GM_\Theta}{r^2}\right)}-\sqrt{\left(\frac{2e}{m_i}\right)r\left(\partial_r\phi\right)}\right]+n_e e\sqrt{\left(\frac{2e}{m_e}\right)r\left(\partial_r\phi\right)}. \tag{2.20}$$

In order for the numerical characterization, we express the above SWP governing equations in a time-stationary (steady-state) normalized form. The normalization scheme here is the same as that of the previous SIP scale. Accordingly, the normalized forms of equations (2.15) - (2.20) can, respectively, be expressed as

$$N_e = \left[1-\left(\frac{2}{2\kappa-3}\right)\Phi\right]^{-\kappa+1/2}, \tag{2.21}$$

$$M\left(\partial_\xi N\right)+N\left(\partial_\xi M\right)+\left(\frac{2}{\xi}\right)M\,N=0, \tag{2.22}$$

$$M\left(\partial_\xi M\right)=-T_e^*\left(\partial_\xi\Phi\right)-\left(\frac{\alpha\lambda_J\Gamma n_0^{\Gamma-1}}{m_i c_s^2}\right)N^{\Gamma-2}\left(\frac{2\kappa-1}{2\kappa-3}\right)\left[1-\left(\frac{2}{2\kappa-3}\right)\Phi\right]^{-\kappa-1/2}\frac{1}{\lambda_J}\left[\partial_\xi\Phi+T_e^*\Phi\,\partial_\xi\left(\frac{1}{T_e^*}\right)\right], \tag{2.23}$$
$$-\frac{1}{N}\left[T_i^*\left(\partial_\xi N\right)+N\left(\partial_\xi T_i^*\right)\right]\left[1+\ln\left(N\right)\right]-T_i^*\frac{1}{N}\left(\partial_\xi N\right)-\left(\frac{1}{c_s^2\lambda_J}\right)\frac{GM_\Theta}{\xi^2}+\left(\frac{\eta}{m_i n_0 c_s\lambda_J}\right)\frac{1}{\xi^2}\frac{1}{N}\left[\partial_\xi\left(\xi^2\,\partial_\xi M\right)\right]$$

$$P_T^* = \left(\frac{\alpha\, n_0^\Gamma}{P_0}\right)\left[1-\left(\frac{2}{2\kappa-3}\right)\Phi\right]^{(-\kappa+1/2)\Gamma}+P_{Th}^*\left[1+ln\left(N_i\right)\right]+\beta_0\left(B^*\right)^2, \tag{2.24}$$

$$N_e-N_i=\left(\frac{\lambda_{De}}{\lambda_J}\right)^2\left[\partial_\xi^2\Phi+\left(\frac{2}{\xi}\right)\partial_\xi\Phi\right], \tag{2.25}$$

$$J_{SWP}=N\left[-\sqrt{2\,\xi\left(\frac{1}{c_s^2\lambda_J}\right)\frac{GM_\Theta}{\xi^2}}-\sqrt{\left\{2\left(\frac{T_e}{T_i}\right)\xi\left(\partial_\xi\Phi\right)\right\}}+\sqrt{\left\{2\left(\frac{m_i}{m_e}\right)\left(\frac{T_e}{T_i}\right)\xi\left(\partial_\xi\Phi\right)\right\}}\right]. \tag{2.26}$$

We now couple the above equations to have a set of first-order time-stationary differential equations governing the κ-modified equilibrium GES structure. The RK-IV method is systematically applied for the SWP numerical analysis to proceed with the SIP-derived initial input multi-parametric values [17], as enlisted in Table 2.3 above.

2.3 RESULTS AND DISCUSSIONS

To depict the Sun and its ambient atmosphere with our proposed plasma-based GES-model, we first observe the formation of the SSB with the help of the gravito-electrostatic force balancing. Consequently, we study the strength variation of the self-gravitational field and the electric field with the Jeans-normalized heliocentric radial

distance (radius) for different electron non-thermal plasma environments, indicated by κ as in figure 2.1. Here, the spatial grid size used is 0.10. It is seen that the spherically symmetric plasma mass gets bounded with the SSB so developed. Interestingly, the SSB drifts inward with a higher degree of the electron non-thermality (lower κ-value). For the classical Maxwell–Boltzmann electron distribution, the SSB forms at a radial distance of 3.5 on the Jeans scale. This is in full agreement with the previously reported original GES-model picture [17] affirming the fair reliability of our proposed model.

The inward drifting behaviour of the SSB with greater electron non-thermality can be well explained by looking into the variation of collisional nature of the electrons with varying non-thermality [23]. For high values of κ, the electrons reach a near-Boltzmann distribution. As a result, their possibility of collision with the background lying inertial ions increases. Consequently, the electrons collectively share their thermo-mechanical energy efficiently with the cold ions, initially having low kinetic energy against the electrons. At the same time, the possible role of magnetic fields must also be noticed. The high acceleration of the ions along their possible directional motion increases the magnetic dipole strength. As a result, the magnetic repulsion between these field lines as well as the fields caused due to the local dynamo action increases, causing high magnetic pressure. These effects consequently result in an increase in the bounded solar plasma volume. It is also marked that the SSB-drift is highly sensitive towards lower κ. The difference in the SSB-drifting nature becomes less prominent towards high-electron thermality regime ($\kappa \rightarrow \infty$) than that in low-electron thermality end ($\kappa \rightarrow 3/2$).

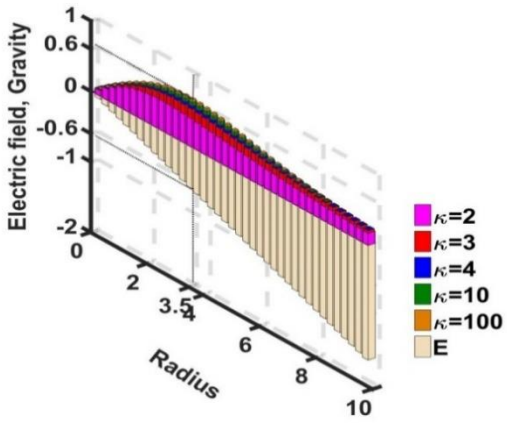

Figure 2.1: *Variation of the normalized value of electric field (E) and self-gravitational field strength (gravity) with the Jeans-normalized heliocentric radial distance for different degrees of the electron non-thermality (as indicated with κ).*

After the above analytic developments, we illustratively discuss the various investigated properties of the bi-scaled equilibrium solar plasmas in two separate subsections as represented below.

2.3.1 SIP CHARACTERIZATION

In order to explore the SIP system, we study the various plasma properties numerically as an integrated model system obtained from the model governing equations (equations (2.8) – (2.14)) in a closed form with the conditions in Table 2.3 as follows.

As depicted in figure 2.2, we show the profile structures of the normalized SIP electric potential with the Jeans-normalized heliocentric radial distance for different κ-values sensibly borrowed from the literature [23]. It is observed from here that the electric potential is independent of the electron non-thermality effects. Due to a very high concentration near the heliocentric region, the electrostatic effects of the positive charge of the plasma constituents are well shielded by the negative charge of the electrons, resulting in negligible potential effects from the polarization perspective. In contrast, as we move away from the centre outwards, the electrostatic effect becomes more prominent due to the increase in diffusivity of the plasma constituent species.

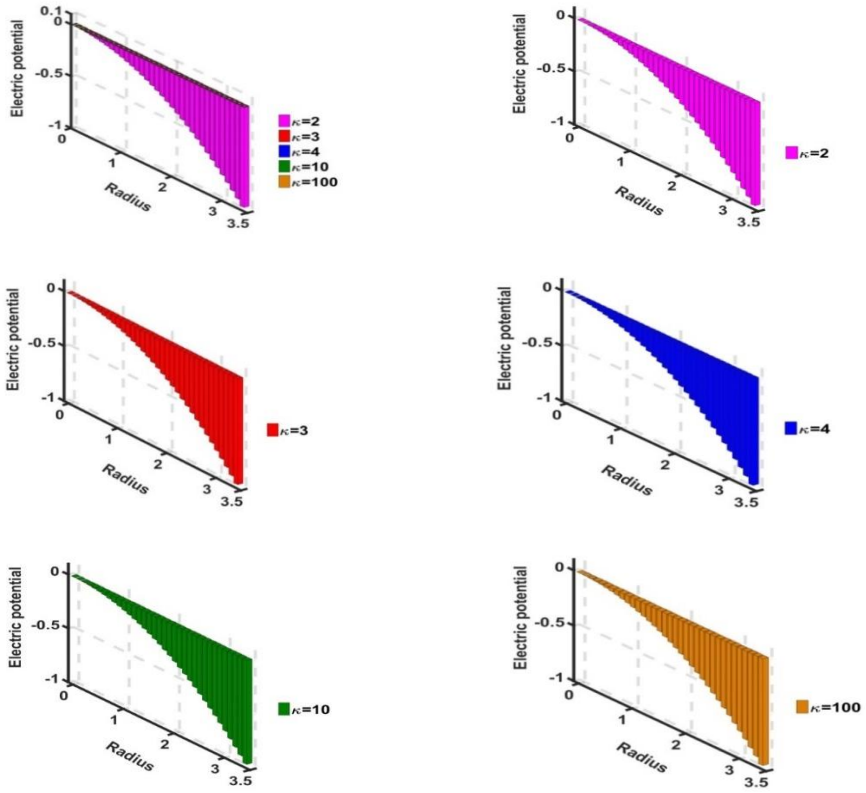

Figure 2.2: *Variation of the normalized SIP electric potential with the Jeans-normalized heliocentric radial distance for different κ-values.*

As depicted in figure 2.3, we plot the spatial profile of the SIP ion Mach number for different κ-values. It is seen that the SIP Mach number increases with an increase in κ. This behaviour is again attributable to the collisional nature of the electrons. For high κ-values, the electrons can effectively transfer their thermo-mechanical energy to the inertial ions to attain high kinetic energy, which in turn results in high Mach value and vice-versa. It is also noticed that the Mach number is highly sensitive to the κ-variation towards lower κ-value. The difference in the Mach number κ-sensitivity becomes less prominent towards the high-electron thermality regime ($\kappa \rightarrow \infty$) than that in the low-electron thermality regime ($\kappa \rightarrow 3/2$).

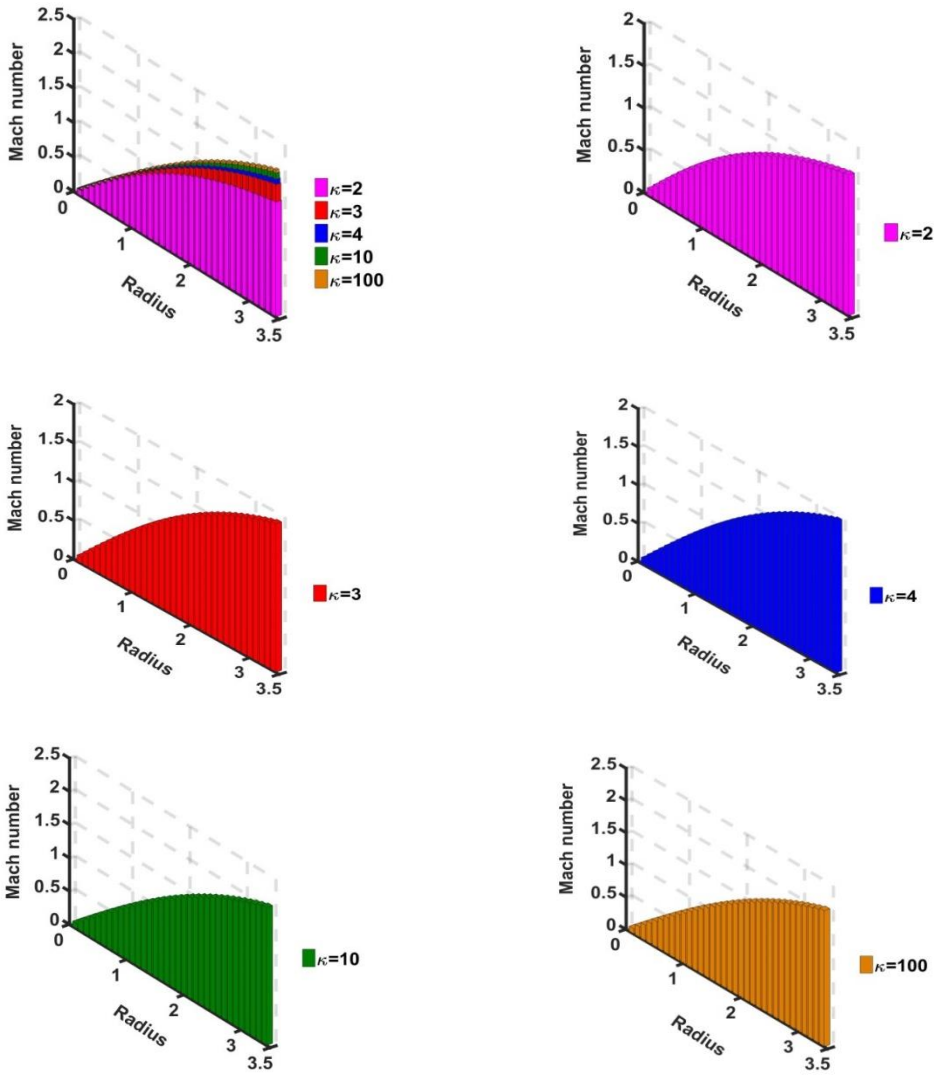

Figure 2.3: *Variation of the SIP ion Mach number with the Jeans-normalized heliocentric radial distance for fixed $T_e/T_i = 1$ and different κ-values.*

In figure 2.4, we present the similar profile as in figure 2.3, but for different values of the electron-to-ion temperature ratio (T_e/T_i) with a fixed κ-value. It is seen that the ion flow speed is independent of this relative temperature for a fixed κ-value. The Mach number reaches almost zero value in the near-heliocentric region due to very high density and strong self-gravity in the core. The Mach number acquires a significant value away from the core outwards where the corresponding plasma density reduces gradually.

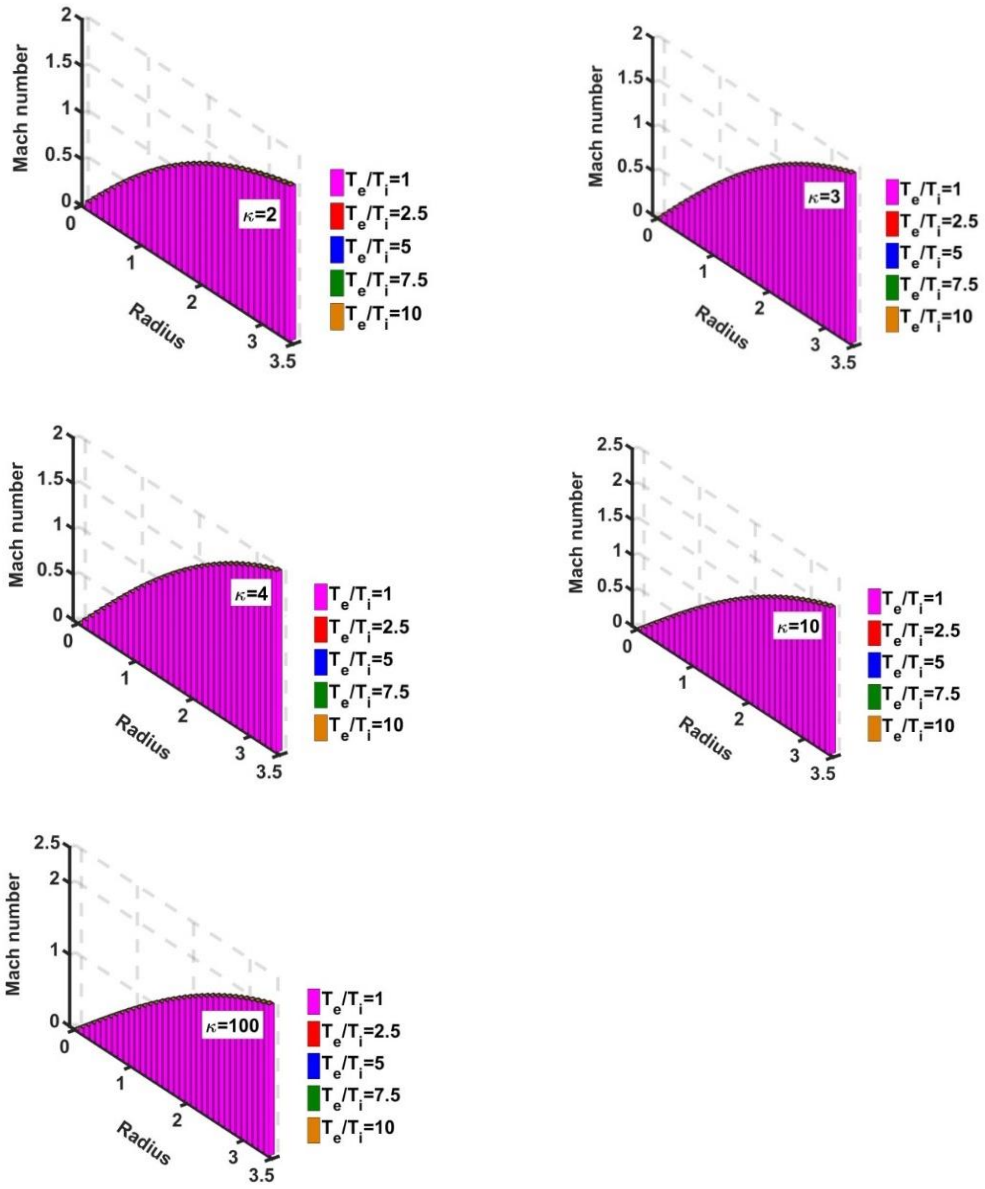

Figure 2.4: *Variation of the SIP ion Mach number with the Jeans-normalized heliocentric radial distance for fixed κ and different T_e/T_i - values.*

As represented in figure 2.5, we depict the spatial profile of the Bohm-normalized SIP current density for different κ-values. It is seen that the current magnitude increases with an increase in κ. The underlying mechanisms behind are the same as that of the Mach number variation with κ. It is also seen that the current density is highly sensitive to κ towards the lower κ-value. The difference in this κ-sensitivity becomes less prominent towards the high-electron thermality regime ($\kappa \to \infty$) than that in the low-electron thermality regime ($\kappa \to 3/2$).

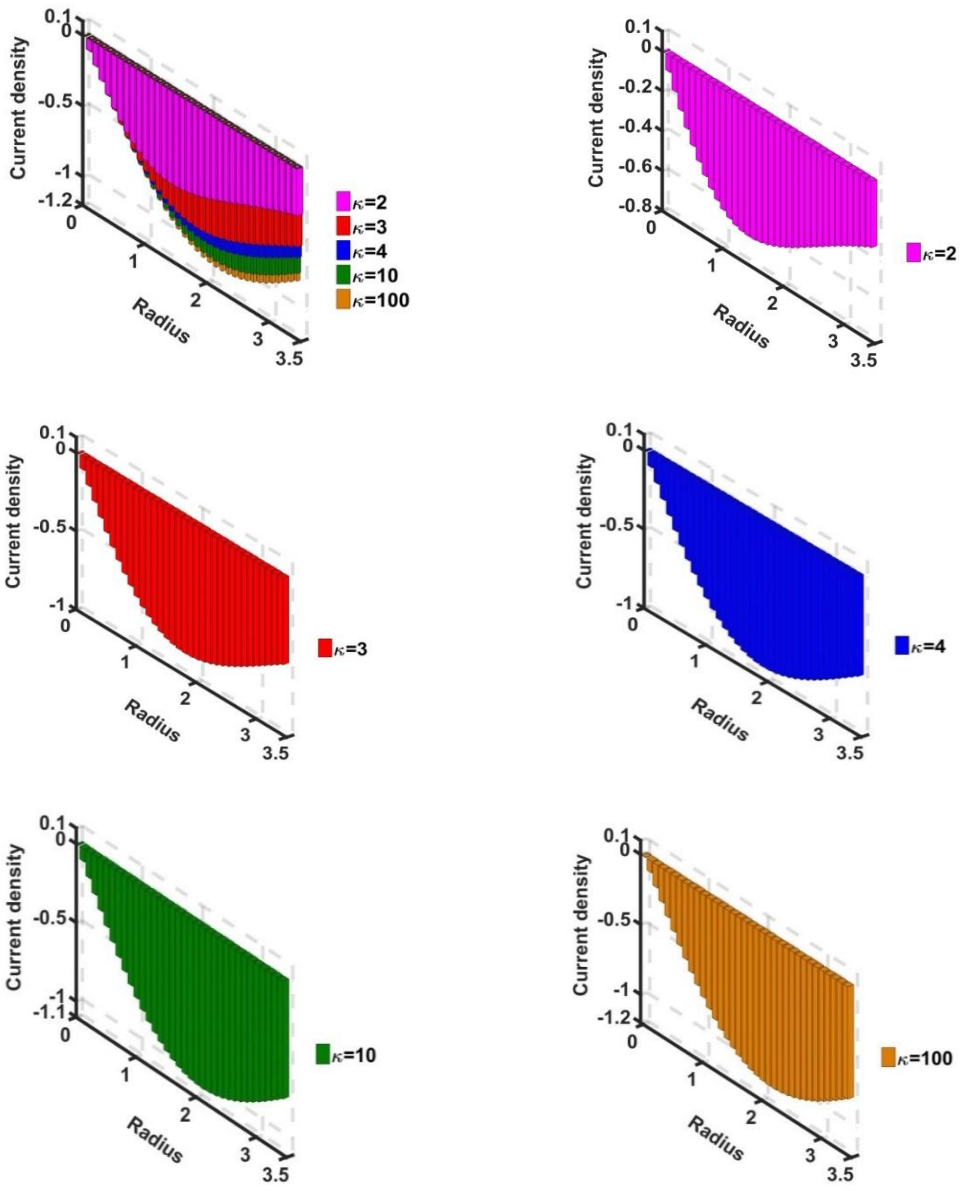

Figure 2.5: *Variation of the normalized SIP current density with the Jeans-normalized heliocentric radial distance for fixed $T_e/T_i = 1$ and different κ-values.*

In figure 2.6, we present the same as in figure 2.5, but for different T_e/T_i - values for a specific electron non-thermality value characterizing a specific case. The current density trend is found to be independent of the T_e/T_i -value. It happens physically due to the fact that the gravito-thermal coupling between the lighter electrons and heavier ions does not affect the interior evolution of the bounded SIP system unless the SSB-zone is reached. In other words, the T_e/T_i - independency of the current density happens actually owing to the fact that the lighter electrons and heavier ions are not gravito-thermally well-coupled to affect the entire SIP system extended from the core to the SSB outwards.

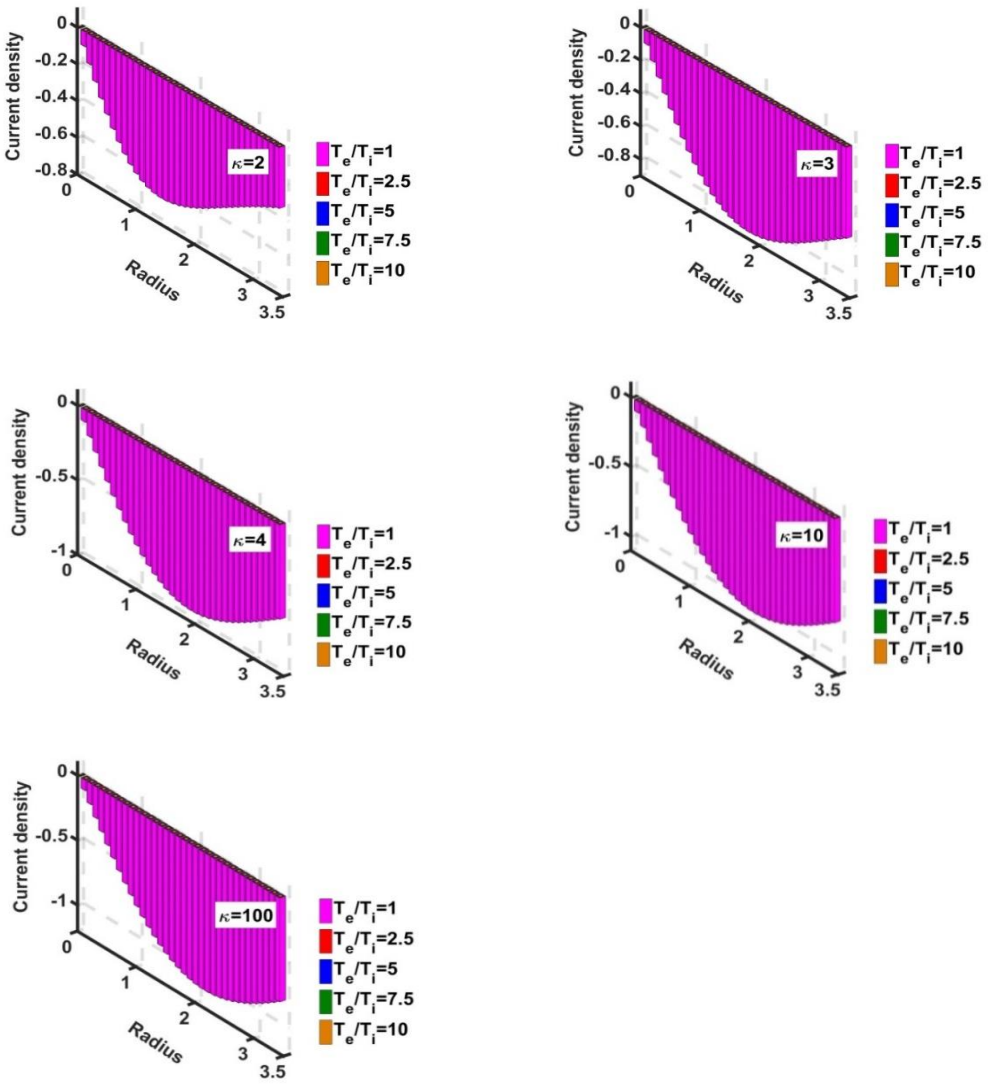

Figure 2.6: *Variation of the normalized SIP current density with the Jeans-normalized heliocentric radial distance for fixed κ and different T_e/T_i –values.*

In figure 2.7, we depict the profile of the Bohm-normalized SIP electric current density with the normalized electric potential for different κ-values. It is again observed that the current density variation with the potential is highly sensitive to κ towards lower κ-value. The difference in this κ-sensitivity becomes less prominent towards the high-electron thermality end ($\kappa \to \infty$) than that in the low-electron thermality end ($\kappa \to 3/2$).

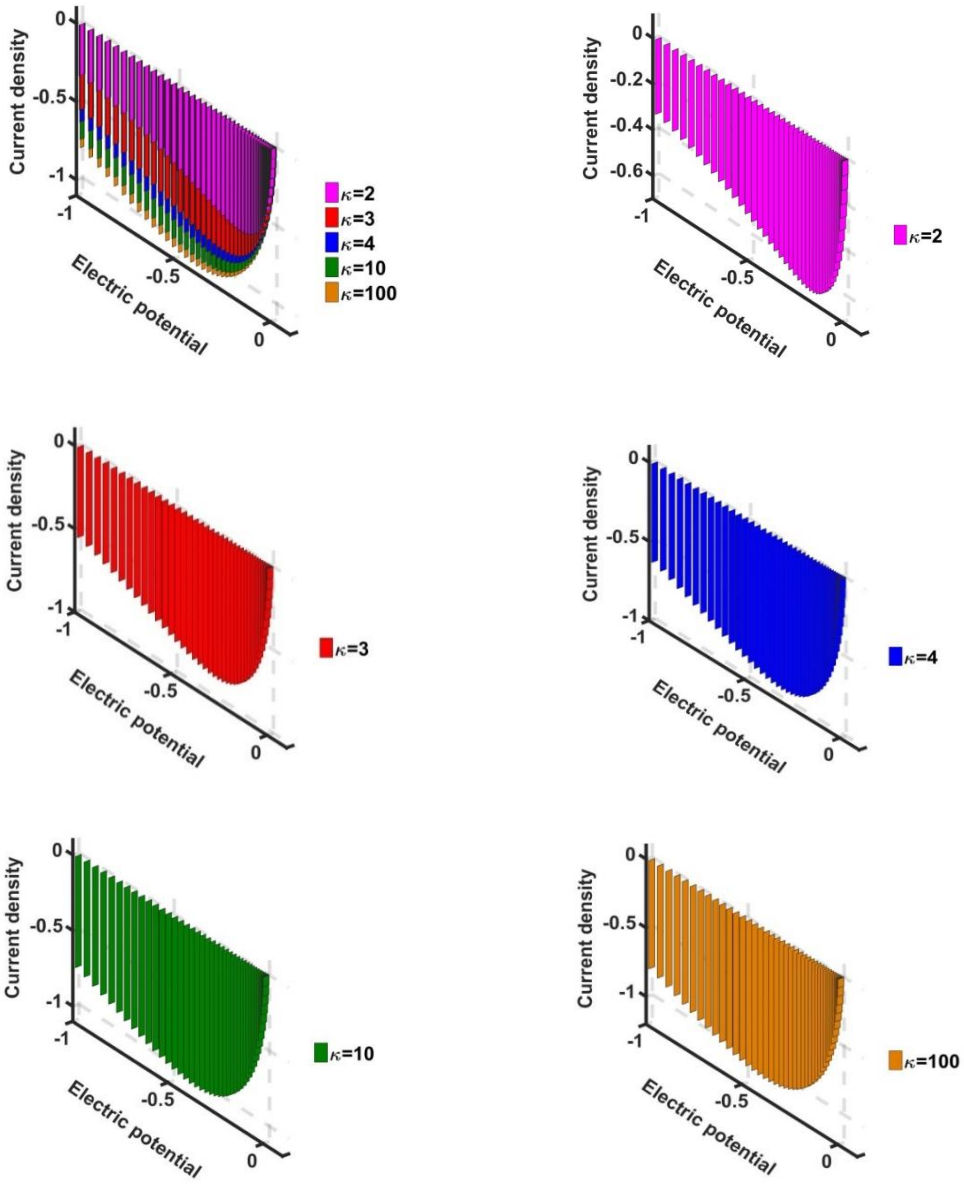

Figure 2.7: *Variation of the normalized current density with the normalized electric potential for fixed $T_e/T_i = 1$ and different κ-values in the SIP.*

In figure 2.8, we show the similar profile as in figure 2.7, but for different T_e/T_i -values for a particular κ-value. It is again seen that this variation is independent of the T_e/T_i -value. The rest on the graphical features here are the same as that in figure 2.6.

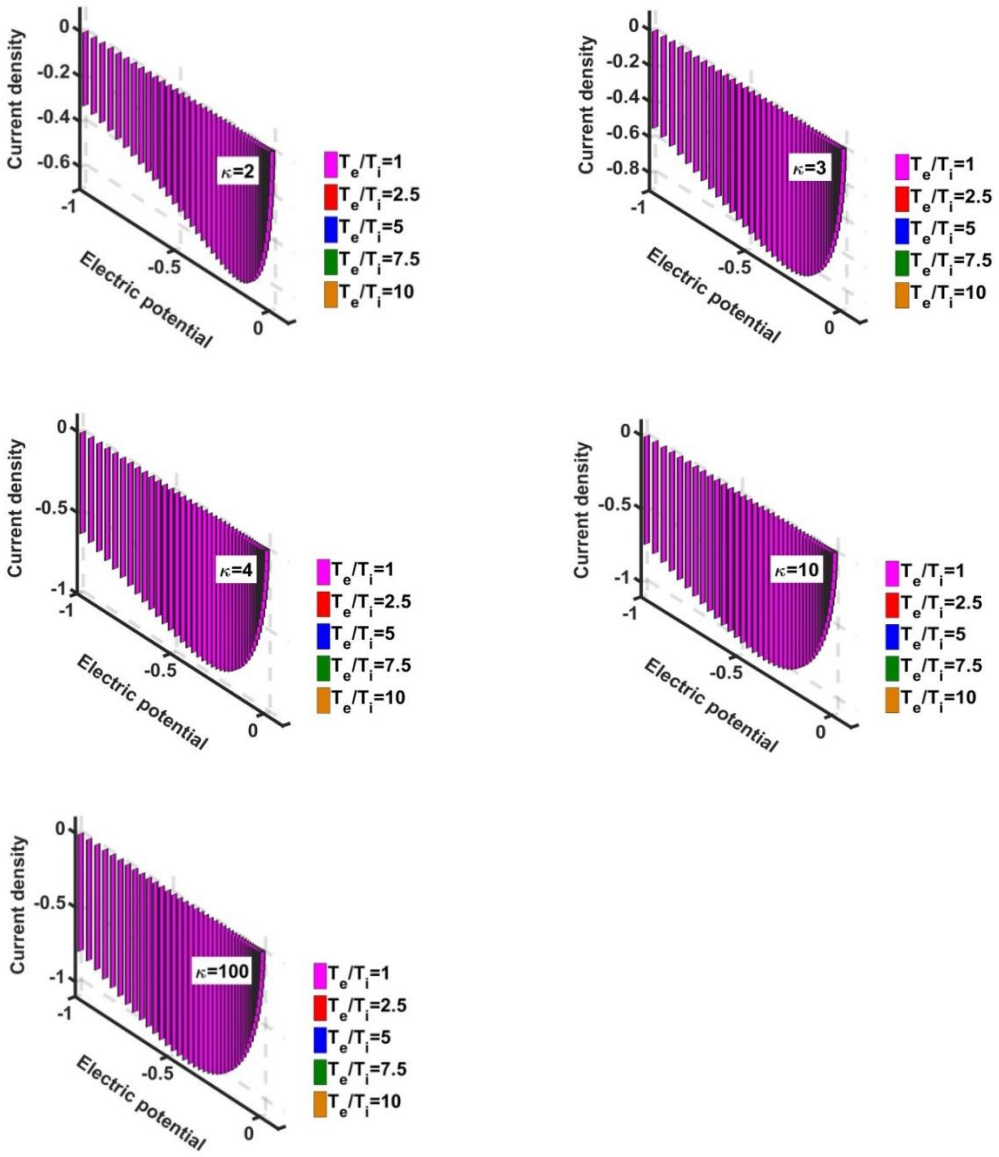

Figure 2.8: *Variation of the normalized current density with the normalized electric potential for fixed κ and different T_e/T_i –values in the SIP.*

2.3.2 SWP CHARACTERIZATION

In order to investigate the SWP system characteristics as in the SIP case already explored above, we study the various equilibrium properties numerically on the basis of the obtained model governing equations (equations (2.21) – (2.26)) as follows.

As shown in figure 2.9, we get the profile of the normalized SWP electric potential with the Jeans-normalized heliocentric radial distance for different κ-values. Here, the spatial grid size used is 20. Clearly, the potential is independent of the electron non-thermality extent. Due to high plasma concentration in the SIP zone, the positive charge effect is well shielded by the negative electrons, resulting in the low electrostatic effect. As the observer moves away from the near-SIP zone, due to the increase in diffusivity of the medium, the potential becomes more prominent in the far-SIP zone.

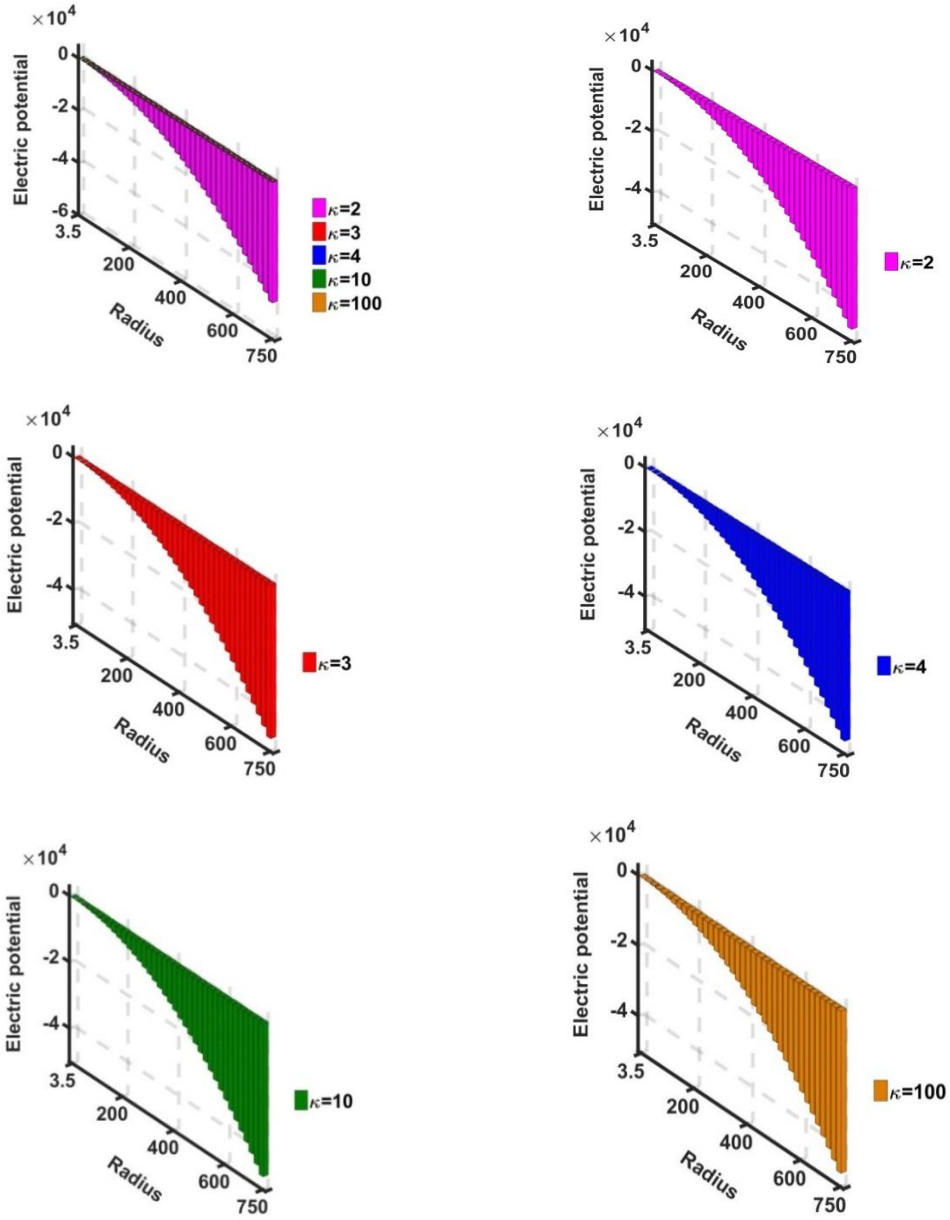

Figure 2.9: *Variation of the normalized SWP electric potential with the Jeans-normalized heliocentric radial distance for different κ-values.*

In figure 2.10, we depict the spatial profile of the SWP Mach number for different κ-values. It is seen that the Mach number is almost insensitive to the κ-variation, except towards the high electron non-thermality corner. The collision of ions with electrons energizes these ions to the extent of dispersion from the directional motion, except for the highly non-thermal electrons with very low collision probability. The diffuse SWP magnetic field structure may also be an active agent to accelerate the SWP ionic flow dynamics.

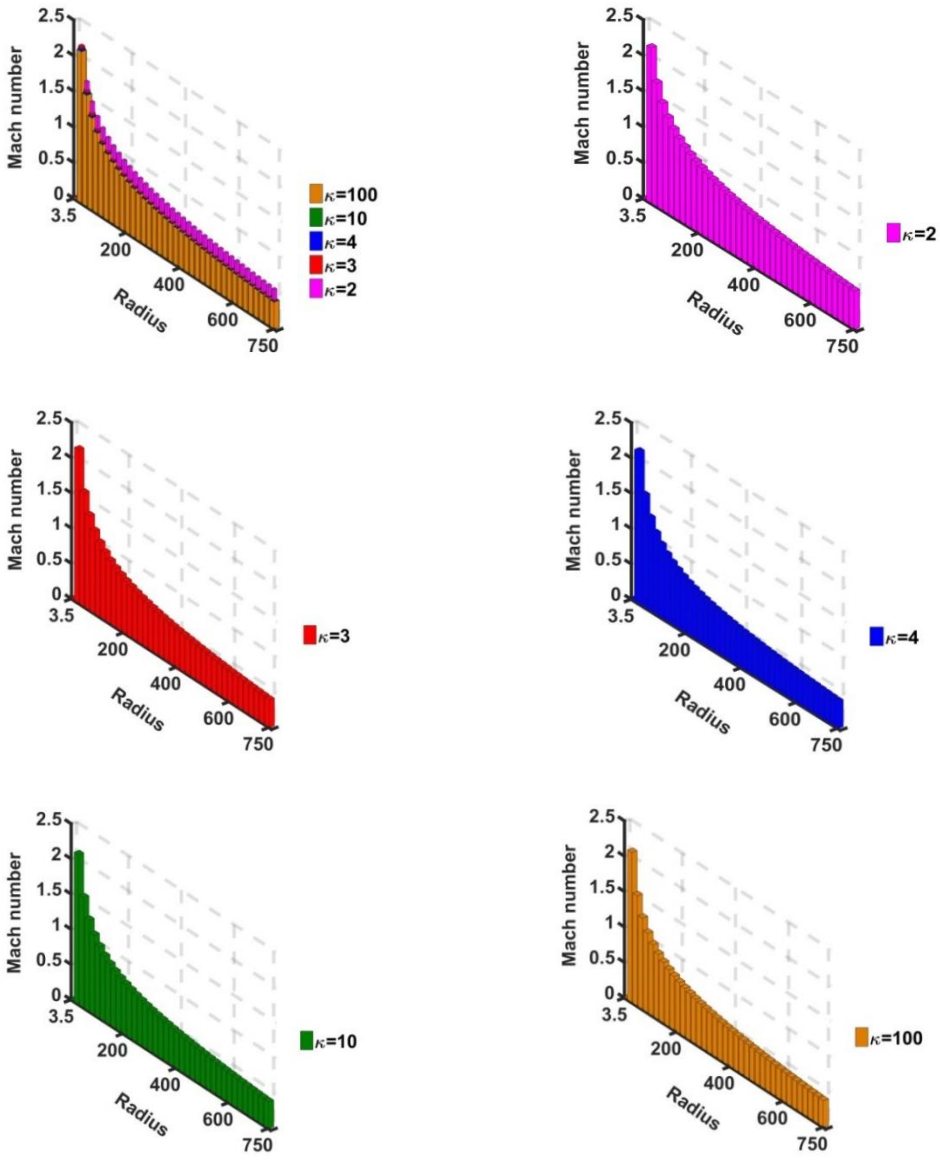

Figure 2.10: *Variation of the SWP ion Mach number with the Jeans-normalized heliocentric radial distance for fixed T_e/T_i = 1 and different κ-values.*

In figure 2.11, we present the similar profiles as in figure 2.10, but for different T_e/T_i - values. It is seen that the ion flow speed is independent of this relative temperature for a particular fixed κ-value. It physically indicates that the gravito-thermally coupled electron-ion thermodynamics does not effectively influence the radial outflow of the quasi-neutral SWP (against the κ-sensitivity of the flow dynamics as seen in figure 2.10).

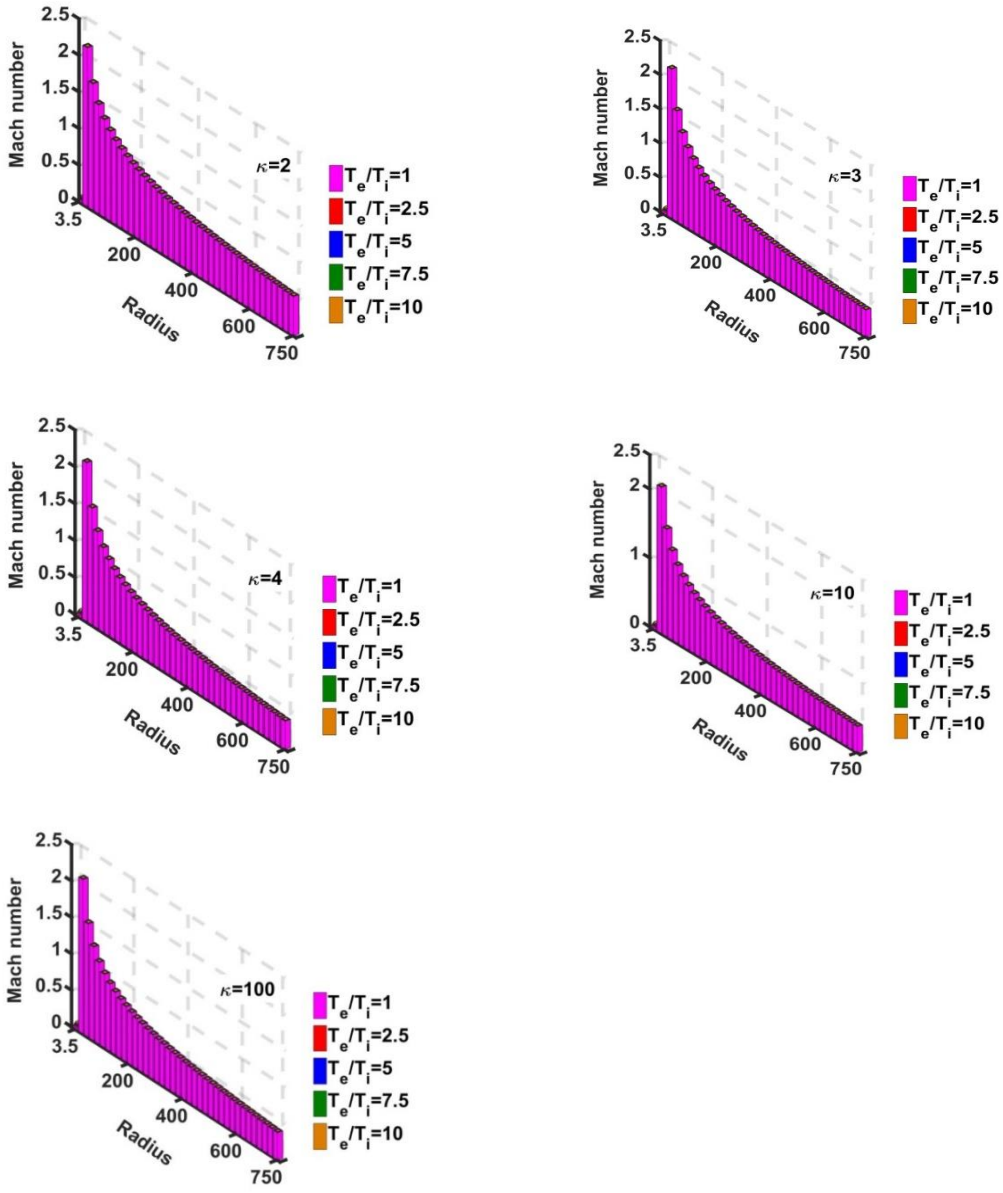

Figure 2.11: *Variation of the SWP ion Mach number with the Jeans-normalized heliocentric radial distance for fixed κ and different T_e/T_i – values.*

As in figure 2.12, we show the spatial profile of the Bohm-normalized SWP current density for different κ-values. It is seen that the magnitude of the SWP current

density is insensitive to κ. The current density reaches a peak-value in the near-SIP zone. It is negligible as the observer moves away from the SIP. The underlying mechanism behind it may be the appearance of an effective net charge dispersion caused against the directional motion of the constitutive solar plasma species.

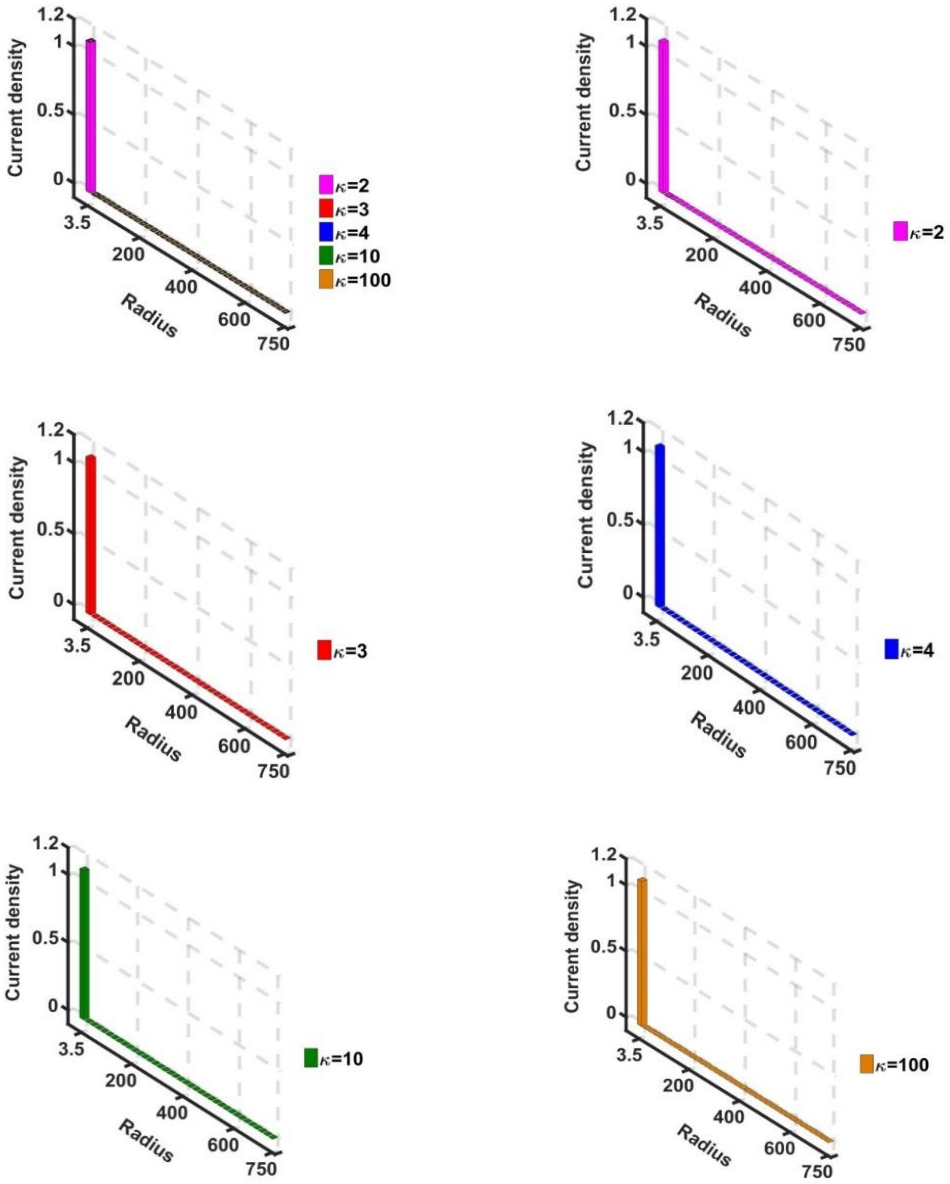

Figure 2.12: *Variation of the normalized SWP electric current density with the Jeans-normalized heliocentric radial distance for fixed T_e/T_i = 1 and different κ-values.*

As depicted in figure 2.13, we represent the similar profile as in figure 2.12, but for different T_e/T_i - values for a particular κ-value. It is seen that in the near-SIP zone, the current density is highly sensitive to this temperature ratio. As electron temperature

increases (or ion temperature decreases), the current density also increases for a particular κ-value. It may be due to high thermal energy transferability of the electrons to the cold ions with an increase in the electron temperature (or decrease in the ion temperature), only in the near-SIP zone of the infinite SWP.

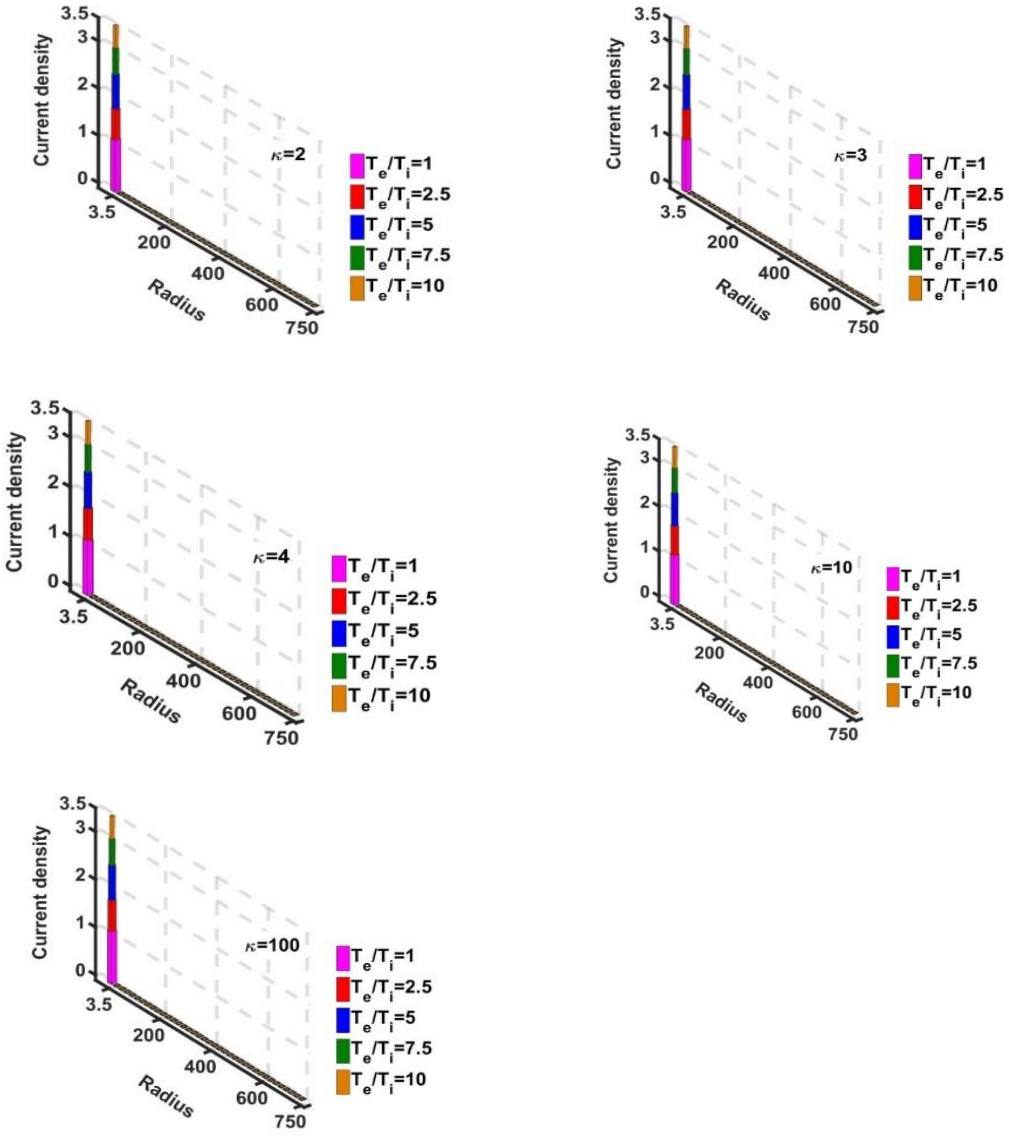

Figure 2.13: *Variation of the normalized SWP electric current density with the Jeans-normalized heliocentric radial distance for fixed κ and different T_e/T_i – values.*

In figure 2.14, we depict the profile of the Bohm-normalized SWP electric current density with the normalized electric potential for different κ-values. It is seen that the SWP current density variation with the potential is insensitive to the κ-variation.

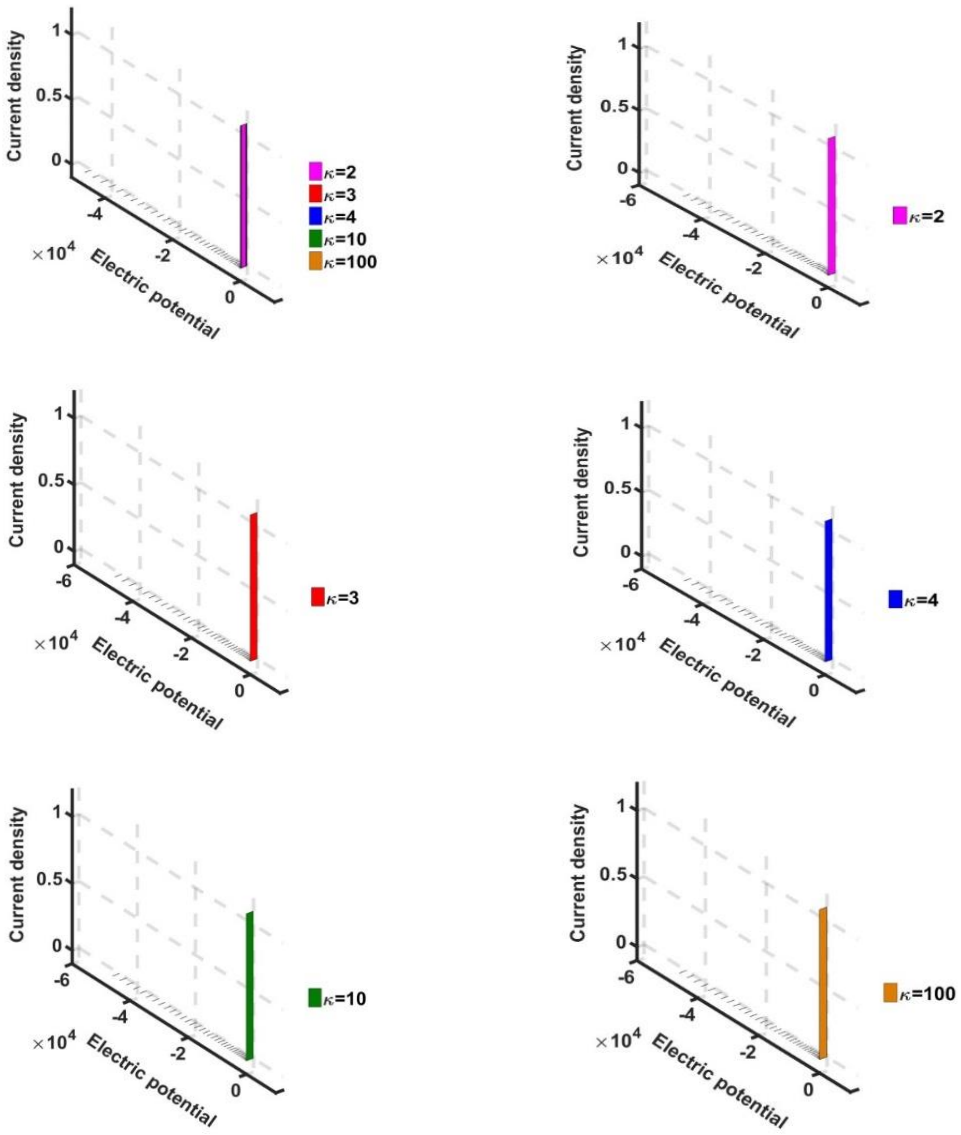

Figure 2.14: *Variation of the normalized electric current density with the normalized electric potential for fixed $T_e/T_i = 1$ and different κ-values in the SWP.*

In figure 2.15, we represent the similar profile as that in figure 2.14, but for different T_e/T_i - values, for a particular κ-value. It is seen that the SWP current density is positively sensitive to increase in electron temperature (or decrease in ion temperature), only near the zero value of the electric potential for any electron non-thermality extent.

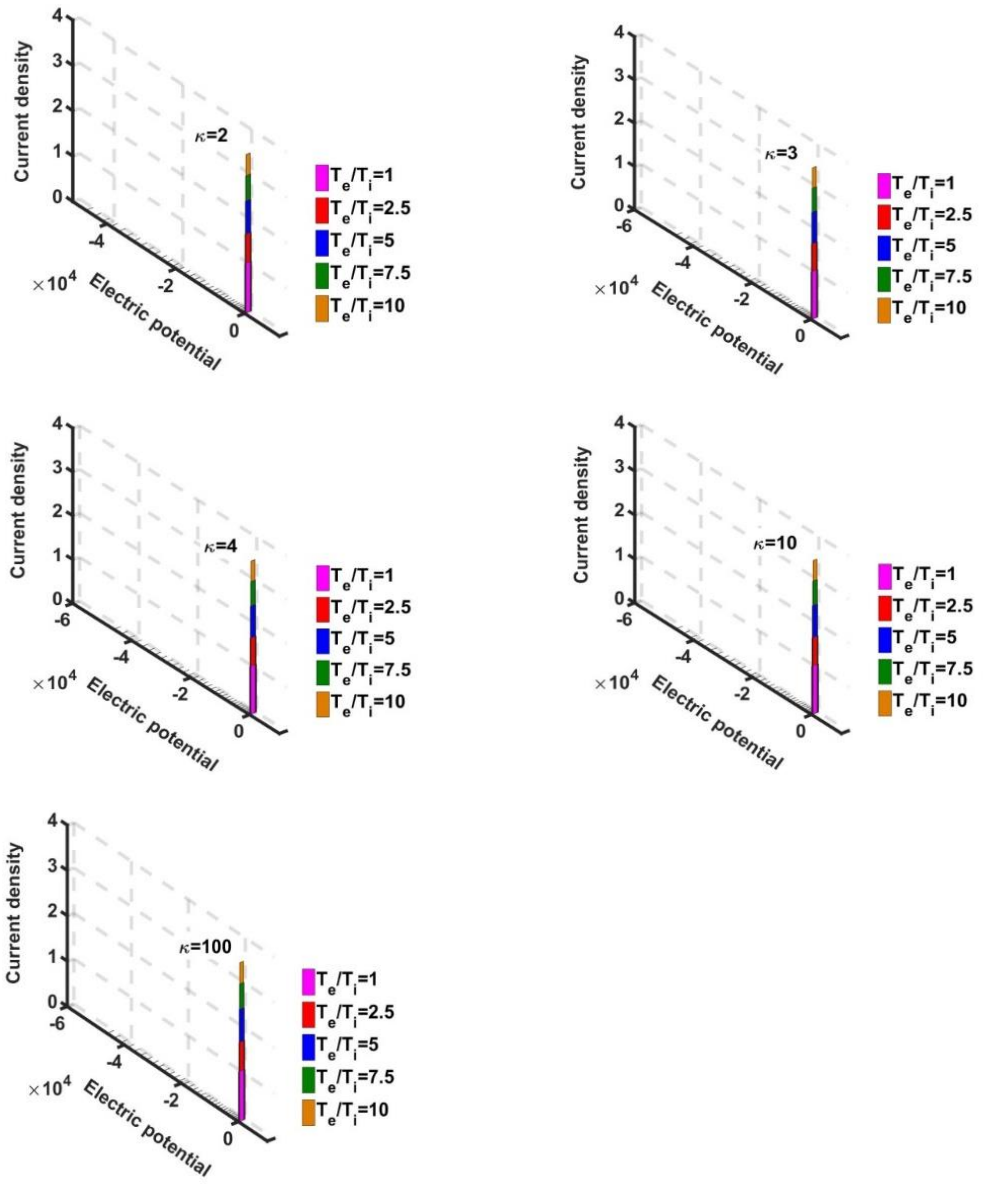

Figure 2.15: *Variation of the normalized electric current density with the normalized electric potential for fixed κ and different T_e/T_i – values in the SWP.*

In the above analyses, we see that our study reveals the *κ*-sensitiveness of various solar plasma structuring parameters. It qualitatively signifies the response of the parameter to the variation of the electronic non-thermality extent. As *κ* increases, the degree of collision among the constitutive particles increases. The high collision probability of the hot electrons with the cold ions facilitates the electrons to transfer their thermo-mechanical energy efficiently to the inertial cold ions and tends to make the local solar plasma system isothermal. As a result, the sensitivity of a particular parameter to *κ* shows how the parameter gets saturated to its value in isothermal plasma from its value in the non-isothermal one. For most of the parameters, we find that the *κ*-sensitivity is

high towards lower κ-regime (i.e., high electronic non-thermality). As κ increases, they respond almost in the same manner as in the plasma environment of thermal (Boltzmann) constitutive electrons. So, for such a parameter, it has been revealed herewith that the increasing electron–ion collision (i.e., increasing κ) tends to saturate the parameter towards its isothermal counterpart (i.e., $\kappa \to \infty$).

2.3.3 COMPARATIVE VALUATION

In order for a reliability check-up of the presented model analysis, various properties here can be compared to the realistic scenarios or conventional approaches as follows.

Table 2.4: Present model versus other models

S. No.	Property	Present analysis	Conventional model / experimental values
1	κ-value	We take κ = 2, 3, 4, 10, 100 for analysing the various GES properties covering electron non-thermality levels broadly as per the direct observational data reported elsewhere	Slow solar wind (SW) e^- (Ulysses): 2.71 ± 0.56 [23, 33] Fast SW e^- (Ulysses): 1.90 ± 0.08 [23, 33] Slow SW e^- (Helios): 7.0 ± 1.0 [23, 34] Slow SW e^- (Cluster): 5.0 ± 1.0 [23, 34] Slow SW e^- (Ulysses): 2.4 ± 0.1 [23, 34] Fast SW e^- (Helios): 6.0 ± 0.7 [23, 34] Fast SW e^- (Cluster): 5.00 ± 0.10 [23, 34] Fast SW e^- (Ulysses): 2.30 ± 0.10 [23, 34] Fast SW e^- (Helios/Wind/Ulysses): 5.0 ± 1.5 [23, 35]
2	Mach number	Ion speed in SWP at 1 au is 1.6×10^5 m s^{-1} for κ = 2 (which is in accord with the observations)	Slow SW: speed 2.5×10^5 - 4×10^5 m s^{-1} in the near-Earth space [36] Fast SW: speed 4×10^5 - 8×10^5 m s^{-1} in the near-Earth space [36]
3	Solar surface boundary (SSB)	A non-rigid SSB exists at 3.5 λ_J, i.e., at 7×10^8 m from the heliocenter for the Boltzmann electrons	The solar radius (centre to the photosphere) is estimated to be 6.96×10^8 m [37]

2.4 CONCLUSIONS

This investigation is a continued study on the previously reported idealistic solar plasma-based GES-model, appropriately refined with the proper inclusion of the realistic solar plasma structuring parametric factors. It incorporates the effects of non-thermal (κ-distributed) electron thermo-statistics, global magnetic field, and κ-modified polytropic equation of macroscopic state of a unique type. This new composite equation of state involves the relevant barometric corrections due to the fluid turbulence (logatropic) effects, non- thermal polytropicity, and Lorentz force action simultaneously for the solar plasma description in a real astronomic sense. All the necessary basic governing equations are accordingly developed in a refined form on both the SIP and SWP scales.

An exact numerical analysis of the equilibrium (time-stationary) model equations in a closed form yields an interesting feature of the SIP volume (hence, SSB) showing its shrinking nature with an increase in the electron non-thermality against the thermal GES description, for the first time (figure 2.1). This finding is explicable with the help of collisional nature variation of the electrons with the background ionic fluid for different κ-values. The electric potential variation on both the SIP and SWP scales is found to be independent of the electron non-thermality effects (figure 2.2 and figure 2.9). The entire non-thermal solar plasma flow dynamics is judiciously characterized with the needful graphical description illustratively. It involves the Mach number and electric current density. In the SIP, both the Mach number (figures 2.3-2.4) and current density (figures 2.5-2.6) are sensitive to the electron non-thermality, but insensitive to the relative temperature of the plasma constitutive species. It is found that, on the SWP scale, the Mach number (figures 2.10-2.11) is sensitive to the κ-variation towards the highest electron non-thermality; but, independent of the relative temperature of the plasma constitutive species. In contrast, the current density (figures 2.12-2.13) on the SWP scale is κ-independent; but, sensitively dependent on the relative temperature of the plasma constituents. Lastly, a comparative assessment of the key results of our present model analysis is reliably performed with the previous studies widely reported in the literature.

REFERENCES

[1] Pierrard, V. and Lazar, M. Kappa distributions: theory and applications in space plasmas. *Solar Physics,* 267, 153:153-174, 2010.

[2] Livadiotis, G. and McComas, D. J. Understanding kappa distributions: a toolbox for space science and astrophysics. *Space Science Reviews*, 175:183–214, 2013.

[3] Yoon, P. H., Sarfraz, M., Ali, Z., Salem, C. S., and Seough, J. Proton cyclotron and mirror instabilities in marginally stable solar wind plasma. *Monthly Notices of the Royal Astronomical Society*, 509(4):4736-4744, 2022.

[4] Vidotto, A. A. The evolution of the solar wind. *Living Reviews in Solar Physics*, 18:3(1)-3(86), 2021.

[5] Chapman, S. Notes on the solar corona and the terrestrial ionosphere. *Smithsonian Contributions to Astrophysics*, 2:1(1)-1(14), 1957.

[6] Hundhausen, A. Direct observations of solar-wind particles. *Space Science Reviews*, 8:690-749, 1968.

[7] Hundhausen, A. Composition and dynamics of the solar wind plasma. *Reviews of Geophysics*, 8(4):729-811, 1970.

[8] Parker, E. N. Dynamics of the interplanetary gas and magnetic fields. *Astrophysical Journal*, 128:664-676, 1958.

[9] Echim, M., Lemaire, J., and Lie-Svendsen, Ø. A review on solar wind modeling: kinetic and fluid aspects. *Surveys in Geophysics*, 32:1–70, 2011.

[10] Ockendon, H. and Ockendon, J. R. *Waves and Compressible Flow*. Springer, Berlin, 2004.

[11] Parker, E. N. Dynamical properties of stellar coronas and stellar winds. II. Integration of the heat-flow equation. *Astrophysical Journal*, 139:93-122, 1964.

[12] Parker, E. N. Dynamical theory of the solar wind. *Space Science Reviews*, 4:666-708, 1965.

[13] Chamberlain, J. W. Interplanetary gas. II. Expansion of a model solar corona. *Astrophysical Journal*, 131:47-56, 1960.

[14] Jockers, K. Solar wind models based on exospheric theory. *Astronomy and Astrophysics*, 6:219-239, 1970.

[15] Lemaire, J. and Scherer, M. Kinetic models of the solar wind. *Journal of Geophysical Research*, 76(31): 7479-7490, 1971.

[16] Maksimovic, M., Pierrard, V., and Lemaire, J. On the exospheric approach for the solar wind acceleration. *Astrophysics and Space Science*, 277:181–187, 2001.

[17] Dwivedi, C. B., Karmakar, P. K., and Tripathy, S. C. A gravito-electrostatic sheath model for surface origin of subsonic solar wind plasma. *Astrophysical Journal*, 663:1340-1353, 2007.

[18] Karmakar, P. K. and Dwivedi, C. B. A numerical characterization of the gravito-electrostatic sheath equilibrium structure in solar plasma. *International Journal of Astronomy and Astrophysics*, 1(4):210-231, 2011.

[19] Gohain, M. and Karmakar, P. K. A generalized two-fluid model of plasma sheath equilibrium structure. *EPL*, 112:45002(1)- 45002(6), 2015.

[20] Gohain, M. and Karmakar, P. K. Nonextensive GES instability with nonlinear pressure effects. *Results in Physics*, 8:592-597, 2018.

[21] Karmakar, P. K., Goutam, H. P., Lal, M., and Dwivedi, C. B. Stability analysis of the gravito-electrostatic sheath-based solar plasma equilibrium. *Monthly Notices of the Royal Astronomical Society*, 460:2919–2932, 2016.

[22] Goutam, H. P. and Karmakar, P. K. Turbulent gravito-electrostatic sheath (GES) structure with kappa-distributed electrons for solar plasma characterization. *Solar Physics*, 292:182 (1)-182(12), 2017.

[23] Livadiotis, G. *Kappa Distributions: Theory and Applications in Plasmas*. Elsevier, Amsterdam, 2017.

[24] Abraham, J. B., Owen, C, J., Verscharen, D., Bakrania, M., Stansby, D., Wicks, R. T., Nicolaou, G., Whittlesey, P. L., Rueda, J. A. A., Jeong, S. Y., and Bercic, L. Radial evolution of thermal and suprathermal electron populations in the slow solar wind from 0.13 to 0.5 au: Parker Solar Probe observations. *Astrophysical Journal*, 931:118(1)-118(9), 2022.

[25] Bryant, D. A. Debye length in a kappa-distribution plasma. *Journal of Plasma Physics*, 56(1):87-93, 1996.

[26] Livadiotis, G. On the generalized formulation of Debye shielding in plasmas. *Physics of Plasmas*, 26:050701(1)-050701(5), 2019.

[27] Kasper, J. C., Klein, K. G., Lichko, E., Huang, J., Chen, C. H. K., Badman, S. T., Bonnell, J., Whittlesey, P. L., Livi, R., Larson, D., Pulupa, M., Rahmati, A., Stansby, D., Korreck, K. E., Stevens, M., Case, A. W., Bale, S. D., Maksimovic, M., Moncuquet, M., Goetz, K., Halekas, J. S., Malaspina, D., Raouafi, N. E., Szabo, A., MacDowall, R., Velli, M., Wit, T. D., and Zank, G. P. Parker solar probe enters the magnetically dominated solar corona. *Physical Review Letters*, 127:255101(1)-255101(8), 2021.

[28] Stix, M. *The Sun: An Introduction*. Springer, Berlin, 1991.

[29] Priest, E. *Magnetohydrodynamics of the Sun*. Cambridge University Press, Cambridge, New York, 2014.

[30] Vazquez-Semadeni, E., Canto, J., and Lizano, S. Does turbulent pressure behave as a logatrope? *Astrophysical Journal*, 492:596-602, 1998.

[31] Taruya, A. and Sakagami, M. Gravothermal catastrophe and Tsallis' generalized entropy of self-gravitating systems. *Physica A*, 307(1–2):185-206, 2002.

[32] Sarfraz, M., Lopez, R. A., Ahmed, S., and Yoon, P. H. Electron mirror and cyclotron instabilities for solar wind plasma. *Monthly Notices of the Royal Astronomical Society*, 509(3):3764–3771, 2022.

[33] Maksimovic, M., Pierrard, V., and Riley, P. Ulysses electron distributions fitted with Kappa functions. *Geophysical Research Letters*, 24(9):1151-1154, 1997.

[34] Stverak, S., Maksimovic, M., Travnicek, P. M., Marsch, E., Fazakerley, A. N., and Scime, E. E. Radial evolution of nonthermal electron populations in the low-latitude solar wind: Helios, Cluster, and Ulysses observations. *Journal of Geophysical Research*, 114: A05104(1)-A05104(15), 2009.

[35] Maksimovic, M., Zouganelis, I., Chaufray, J.-Y., Issautier, K., Scime, E. E., Littleton, J. E., Marsch, E., McComas, D. J., Salem, C., Lin, R. P., and Elliott, H. Radial evolution of the electron distribution functions in the fast solar wind between 0.3 and 1.5 AU. *Journal of Geophysical Research*, 110: A09104(1)-A09104(9), 2005.

[36] Kallenrode, M. *Space Physics: An Introduction to Plasmas and Particles in the Heliosphere and Magnetospheres*. Springer, Heidelberg, 2004.

[37] Carroll, W. and Ostlie, D. A. *An Introduction to Modern Astrophysics*. Cambridge, UK, 2017.